

THE OFFICIAL MAGAZINE OF THE OCEANOGRAPHY SOCIETY

Oceanography

CITATION

Lien, R.-C., B. Ma, C.M. Lee, T.B. Sanford, V. Mensah, L.R. Centurioni, B.D. Cornuelle, G. Gopalakrishnan, A.L. Gordon, M.-H. Chang, S.R. Jayne, and Y.J. Yang. 2015. The Kuroshio and Luzon Undercurrent east of Luzon Island. *Oceanography* 28(4):54–63, <http://dx.doi.org/10.5670/oceanog.2015.81>.

DOI

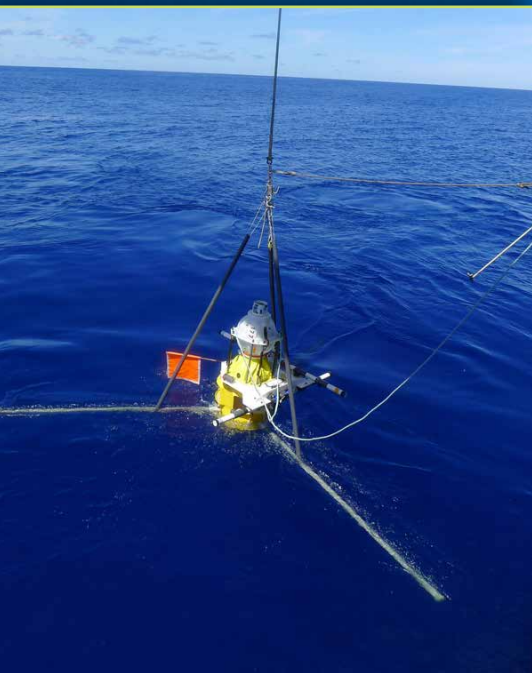
<http://dx.doi.org/10.5670/oceanog.2015.81>

COPYRIGHT

This article has been published in *Oceanography*, Volume 28, Number 4, a quarterly journal of The Oceanography Society. Copyright 2015 by The Oceanography Society. All rights reserved.

USAGE

Permission is granted to copy this article for use in teaching and research. Reproduction, systematic reproduction, or collective redistribution of any portion of this article by photocopy machine, reposting, or other means is permitted only with the approval of The Oceanography Society. Send all correspondence to: info@tos.org or The Oceanography Society, PO Box 1931, Rockville, MD 20849-1931, USA.



The Kuroshio and Luzon Undercurrent East of Luzon Island

By Ren-Chieh Lien, Barry Ma,
Craig M. Lee, Thomas B. Sanford,
Vigan Mensah, Luca R. Centurioni,
Bruce D. Cornuelle, Ganesh Gopalakrishnan,
Arnold L. Gordon, Ming-Huei Chang,
Steve R. Jayne, and Yiing Jang Yang



ABSTRACT. Current structure, transport, and water mass properties of the northward-flowing Kuroshio and the southward-flowing Luzon Undercurrent (LU) were observed for nearly one year, June 8, 2012–June 4, 2013, across the Kuroshio path at 18.75°N. Observations were made from four platforms: an array of six subsurface ADCP moorings, two Seagliders, five pressure inverted echo sounders (PIES), and five horizontal electric field (HEF) sensors, providing the most detailed time series of the Kuroshio and Luzon Undercurrent water properties to date. Ocean state estimates of the western boundary current system were performed using the MIT general circulation model—four-dimensional variational assimilation (MITgcm-4D-Var) system. Prominent Kuroshio features from observations are simulated well by the numerical model. Annual mean Kuroshio transport, averaged over all platforms, is ~16 Sv with a standard deviation ~4 Sv. Kuroshio and LU transports and water mass pathways east of Luzon are revealed by Seaglider measurements. In a layer above the salinity maximum associated with North Pacific Tropical Water (NPTW), Kuroshio transport is ~7 Sv and contains North Equatorial Current (NEC) and Western Philippine Sea (WPS) waters, with an insignificant amount of South China Sea water on the shallow western flank. In an intermediate layer containing the core of the NPTW, Kuroshio transport is ~10 Sv, consisting mostly of NEC water. In the lower layer of the Kuroshio, transport is ~1.5 Sv of mostly North Pacific Intermediate Water (NPIW) as a part of WPS waters. Annual mean Luzon Undercurrent southward transport integrated to 1,000 m depth is ~2.7 Sv with a standard deviation ~2 Sv, carrying solely WPS waters below the salinity minimum of the NPIW. The transport of the western boundary current integrated over the full ocean depth east of Luzon Island is 14 ± 4.5 Sv. Sources of the water masses in the Kuroshio and Luzon Undercurrent are confirmed qualitatively by the numerical model.

INTRODUCTION

The Kuroshio, the primary poleward western boundary current of the northwestern Pacific, is a key component of large-scale ocean circulation and climate variability (Talley et al., 2010). It originates when the North Equatorial Current (NEC) bifurcates east of Luzon, passes Luzon Strait, and flows along the east coast of Taiwan, the continental slope of the East China Sea, and south of Japan (Nitani, 1972). As the Kuroshio flows northward, its transport increases (Andres et al., 2015, in this issue).

Previous studies of the Kuroshio south of Luzon Strait were made primarily by a limited number of shipboard hydrography surveys. East of Luzon Island, immediately north of the NEC bifurcation, a broad range of Kuroshio transport estimates, from 14 Sv to 30 Sv, have been reported (Sverdrup, 1942; Nitani, 1972; Hasunuma and Yoshida, 1978; Qu et al., 1998; Yaremchuk and Qu, 2004). These estimates assume geostrophic balance of the western boundary current (Johns et al., 1989), are sensitive to the assumed

level of no motion (Nitani, 1972), and may have been affected by internal tides and transient eddies during limited shipboard surveys (Qu et al., 1998). Gordon et al. (2014) report on surveys conducted during 2011 and 2012 in Lamon Bay, an embayment within the eastern margin of Luzon (Figure 1). Using meridional velocities recorded by the shipboard acoustic Doppler current profiler (ADCP), they estimate the transport in the upper 600 m crossing 16°30'N and 18°20'N as 9–10 Sv in May 2011 and 14–17 Sv in May 2012, attributing the ~50% increase in 2012 to a southward shift in the NEC bifurcation location, which enriched the Kuroshio with NEC thermocline water while reducing the salinity minimum imprint of the North Pacific Intermediate Water (NPIW; Talley, 1993). Lien et al. (2014) report an annual mean Kuroshio transport of 15 Sv and large transport anomalies of 5–10 Sv due to impinging westward-propagating eddies on a time scale of $O(10)$ days. Previous studies conclude that Kuroshio transport is inversely correlated with the bifurcation latitude of

the NEC (Qiu and Lukas, 1996; J. Yang et al., 2013; Gordon et al., 2014) considering that the bifurcation moves northward in winter and during El Niño events (Kim et al., 2004; Qu and Lukas, 2003).

Earlier studies describe a southward-flowing current beneath the Kuroshio east of Luzon Island—the Luzon Undercurrent (LU; Hu and Cui, 1991; Qu et al., 1997; Hu et al., 2013). LU southward transport is estimated to be 1.0–6.9 Sv with a maximum southward velocity of 0.05–0.28 $m s^{-1}$ (Hu and Cui 1991; Qu et al., 1997). Qu et al. (1998) suggest that the LU transports the low-salinity NPIW southward. Recent work by Mensah et al. (2015) suggests that the NPIW below its salinity minimum is mostly advected southward by the LU, whereas the NPIW above its salinity minimum is advected northward by the Kuroshio.

Temperature, salinity, and velocity measurements of the Kuroshio and the LU east of Luzon Island were made simultaneously for nearly one year by four independent platforms that included moorings, Seagliders, horizontal electric field (HEF) sensors, and pressure inverted echo sounders (PIES). The combination of HEF and PIES is called HPIES. These measurements provide an opportunity to study the transport and water mass properties of the Kuroshio and the LU. The experimental site and observational platforms are described in the next section. Transports and water mass properties are presented. Results of numerical model simulations of Kuroshio and LU transports are presented and compared with observations.

EXPERIMENTAL SITE AND OBSERVATIONAL PLATFORMS

A US–Taiwan collaborative field experiment entitled Origins of Kuroshio and Mindanao Currents/Observations of Kuroshio Transports and their Variability (OKMC/OKTV) was conducted in 2011–2013 to study the western boundary current in the western Pacific Ocean (Rudnick et al., 2011; Jan et al., 2015). Primary scientific goals of the OKMC/OKTV

experiment include studying the variability of Kuroshio properties and improving predictions of Kuroshio circulation near its origin. An observational experiment was designed to measure Kuroshio properties upstream of Luzon Strait, and numerical model simulations of the current are performed to compare with observations. Based on historical drifter velocity data (Centurioni et al., 2004) and AVISO (Archiving, Validation, and Interpretation of Satellite Oceanographic data) surface currents (not shown), the experiment site was located along 18.75°N (Figure 1). Here, the Kuroshio is well organized and flows northward east of Luzon Island.

Platforms deployed at the experiment site (Figure 2a) included six subsurface moorings spaced roughly 16 km apart along 18.75°N in a zonal section between 122°E and 122.87°E and spanning ~80 km

at the Kuroshio entrance to Luzon Strait. Each mooring was equipped with one upward-looking 75 kHz ADCP at 450 m nominal depth. The ADCP recorded averaged velocity measurements every 15 min in 8 m vertical bins between 450 m and 45 m depth over the period June 2012–May 2013. The uncertainty of ADCP velocity measurements is $\sim 2.5 \text{ cm s}^{-1}$.

Two Seagliders collected time series of high-resolution sections along the mooring line over the period November 2012 to May 2013 (Figure 2a). Seaglider is a buoyancy-driven, long-range autonomous underwater vehicle designed for oceanographic research (Eriksen et al., 2001). Each Seaglider was equipped with a Sea-Bird conductivity-temperature-depth (CTD) sensor that sampled temperature and salinity every 8 s while profiling to 1,000 m at $\sim 0.5 \text{ m s}^{-1}$. The Seagliders made 15 sections between

121.8°E and 123.2°E nominally at 18.75°N. Depth-average currents (V_{dac}) were calculated from the difference between GPS-derived surface positions at the start and end of a dive, combined with a hydrodynamic model of glider motion. Geostrophic shear was calculated and converted to absolute geostrophic velocity using V_{dac} (Lien et al., 2014; K.-C. Yang et al., 2015, in this issue).

Four HPIES were deployed along 18.75°N and one HPIES at $\sim 30 \text{ km}$ north of the center of the moored array (Figure 2a). HPIES integrates the HEF and PIES sensors on a bottom lander (Meinen et al., 2002). HEF measures the electric field due to the vertically averaged motion of seawater through Earth's magnetic field (Sanford, 1971; Chave and Luther, 1990). The depth-averaged velocity is inferred from the measured electric field. PIES measured bottom pressure and round-trip acoustic travel time τ between the ocean bottom and sea surface (Watts and Rossby, 1977). Aided by in situ CTD observations, the gravest empirical mode (GEM) provides lookup tables for the conversion of τ into full-depth hydrographic profiles (Meinen and Watts, 2000; Sun and Watts, 2001; Watts et al., 2001). The GEM used in this analysis is built from a composite of shallow (down to 1,000 db) hydrographic casts collected by the two Seagliders and deep casts obtained from the National Oceanographic Data Center (NODC) spanning 1975–2012 within 18.67°N–19.25°N, 121.67°E–123.5°E. A synthetic τ is calculated from observed hydrographic profiles of 0–800 db, called τ_{800} . The reference depth of 800 db is chosen because most Seaglider dives reach this depth. A GEM lookup table is established between τ_{800} and specific volume anomaly vertical profiles (Meinen and Watts, 2000). The GEM method captures 82.3% of the variance of observed temperature variation in the upper 800 m. The PIES τ data are converted to τ_{800} and objectively mapped following Donohue et al. (2010). The GEM lookup table provides estimated profiles of specific

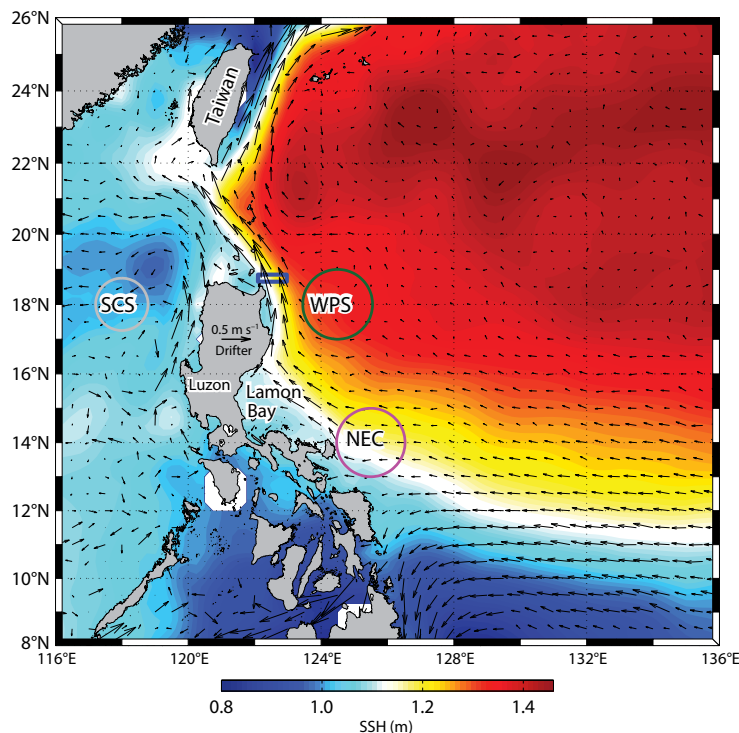


FIGURE 1. AVISO sea surface height (SSH; color shading) averaged between June 2012 and May 2013 and historical Lagrangian drifter-measured horizontal current at 10 m depth averaged between 1984 and 2014 (black vectors). The experimental site for the Origin of Kuroshio and Mindanao Currents (OKMC) program northeast of Luzon Island at the Kuroshio entrance to Luzon Strait is indicated by the blue box. The circles indicate the areas where Argo float data are used to define the temperature-salinity properties of the North Equatorial Current (NEC), West Philippine Sea (WPS), and South China Sea (SCS).

volume anomaly along the array, and the geostrophic shear is calculated. The absolute geostrophic current is obtained using PIES pressure and mooring ADCP velocity measurements following the method described by Andres et al. (2008). The depth-integrated current velocity data derived from PIES is also used to compute the adjustment to HEF from the correlation of horizontal velocity and electrical conductivity (Sanford, 1971). Because the seafloor is volcanic with low electrical conductivity, no adjustment is necessary for the shorting of the bottom sediment.

Velocity derived from 1,760 Lagrangian drifters archived in the Global Drifter Program (GDP) historical database (Niiler, 2001; Maximenko et al., 2013) spanning November 1984 to June 2014 captures the structure of the Kuroshio surface current. As part of the OKMC program, 244 of these drifters were deployed southeast of Taiwan. It has been discovered that archived drifter data contain a large percentage of near-surface velocity measurements erroneously attributed to drogued drifters. The data set used in this work was corrected as described in Lumpkin et al. (2013). The drifter data were further quality controlled for unrealistic locations, and a Kriging interpolation scheme was then applied to obtain a regularly spaced, 6 hr drifter location time series (Hansen and Poulain, 1996) from which the drifters' velocities were obtained using the center difference formula as a proxy for the first time derivative. A further correction of the drifter data was performed at the Lagrangian Drifter Laboratory of the Scripps Institution of Oceanography. A wind slip correction was applied (Niiler et al., 1995), and the velocity data from drifters that had lost their drogues were recovered as described in Pazan and Niiler (2001). The temporal average surface currents are computed from ~30 years of drifter measurements. The drifter velocity vectors reveal the NEC, the Kuroshio, and the semi-permanent anticyclonic recirculation gyre east of the Kuroshio at 20°N–24°N (Figure 1).

KUROSHIO TRANSPORT AND WATER PROPERTIES

Velocity

The mean meridional velocity structure measured by the moored array and Seagliders (Figure 2) shows that the Kuroshio axis (i.e., the position of maximum surface current) is located at ~122.4°E. Lien et al. (2014) report that the Kuroshio axis measured by the mooring varies by less than 10 km through the entire year. The AVISO surface current averaged over the same period reveals the same Kuroshio axis position, but with a much lower magnitude, presumably due to smoothing. The meridional surface current averaged from 437 drifters operating from November 1987 to June 2014 within 1/4° of 18.75°N is nearly the same in magnitude and zonal structure as measured by moorings, suggesting that mooring observations represent the Kuroshio current on average.

A large portion of the Kuroshio is in geostrophic balance with the Rossby number $Ro \sim 0.2$, except in the upper

100 m on the Kuroshio's western flank where $Ro \sim 1$ (Lien et al., 2014). The averaged geostrophic current measured by Seagliders over the period November 2012 to May 2013 agrees reasonably well with the annual mean Kuroshio current measured by the moored array (Figure 2), with rms differences of 0.03 m s^{-1} and 0.1 m s^{-1} on the eastern and western flanks of the Kuroshio, respectively. The greater difference on the western flank is presumably due to the Kuroshio's ageostrophic balance (Lien et al., 2014).

Transport

Kuroshio transport is computed using ADCP velocity measurements from the moored array linearly extrapolated between the surface and 45 m and between 450 m and 600 m (Lien et al., 2014). Integrating all positive northward velocity across the moored array yields Kuroshio transport. Similarly, the northward geostrophic current measured by Seagliders is integrated across each of the 15 Seaglider sections, and the geostrophic

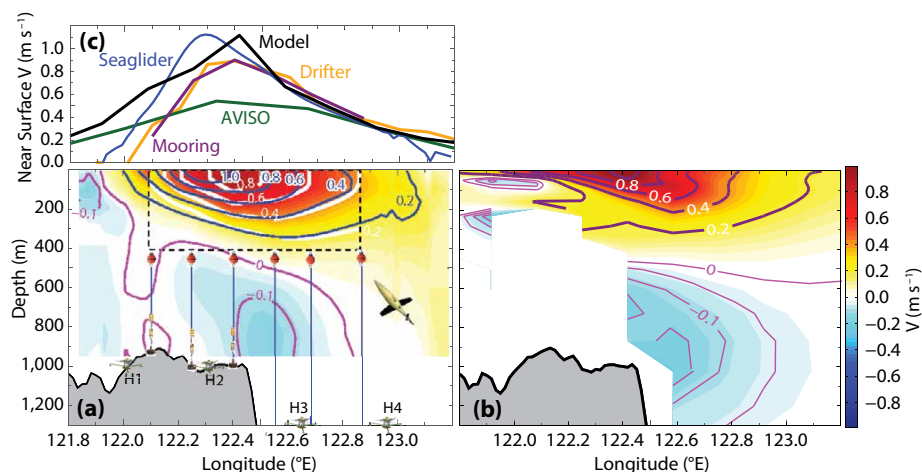


FIGURE 2. Temporal mean of the (a) observed and (b) MITgcm-OKMC optimized model meridional component of velocity of the western boundary current along 18.75°N. In panel (a), color shading and white contour lines within the dashed black box represent the average of the meridional component of the western boundary current from one year of measurements from an array of six subsurface moorings (orange dots and blue vertical lines). The color shading outside the black dashed box represents the geostrophic component of the northward western boundary current averaged from 15 sections of Seaglider measurements during the period November 2012 to May 2013. An image of the Seaglider is shown in (a). Blue and magenta contours represent northward and southward isotachs from Seaglider measurements, respectively. Schematic diagram of HPIES (a combination of horizontal electric field [HEF] sensors and pressure inverted echo sounders [PIES]) and locations are shown in (a), labeled H1–H4. A fifth HPIES (H5) located north of this section is not shown. (c) The near-surface velocity measured by Seagliders (averaged 0–10 m), moorings (averaged 0–10 m), AVISO (surface), drifters (10 m depth), and model simulations (13 m, the shallowest depth). In panels (a) and (b), isotachs are labeled with the unit of m s^{-1} .

northward current estimated from PIES is integrated across the PIES array to yield Kuroshio transport.

Kuroshio transport estimates computed from these three independent platforms have similar temporal fluctuations and magnitudes. Mean and standard deviation estimates of Kuroshio transport from the moored array, Seagliders, and PIES are 15 ± 3 Sv, 18 ± 4 Sv, and 13 ± 4 Sv, respectively (Figure 3). The moored array underestimates the Kuroshio transport by nearly 10% due to the transport beyond the spatial coverage of the array (Lien et al., 2014). Averaging over these three estimates, including the correction of missing transport in the moored array, the annual Kuroshio transport is 16 ± 4 Sv.

Kuroshio transports computed from PIES and Seaglider measurements are in good agreement with transport computed from the moored array measurements, reflecting the near geostrophic balance of the Kuroshio current and the high quality of the geostrophic current estimates from Seaglider and PIES measurements. The major discrepancy between transport estimated by the moored array and that by the PIES during August–September 2012

may be due to the imperfect linear extrapolation of moored measurements, the imperfect GEM model for computing the geostrophic current from PIES measurements, and the ageostrophic balance of the Kuroshio on its western flank. Impinging eddies may modify Kuroshio water mass properties (Early et al., 2011) and therefore the acoustic travel time measurements made by PIES.

Previous studies report that impinging mesoscale eddies modulate Kuroshio transport (Y. Yang et al., 1999; Chern and Wang, 2005; Kuo and Chern, 2011; Chang et al., 2015). Lien et al. (2014) identified and tracked westward-propagating eddies using AVISO sea surface height (SSH) and surface geostrophic current data, and demonstrated that almost all the observed Kuroshio transport anomalies on an intra-seasonal time scale can be explained by impinging eddies. Anticyclonic (cyclonic) eddies increase (decrease) Kuroshio transport. Large transport variations of nearly 10 Sv in $O(10$ days) during June–July 2012 and April–June 2013 (Figure 3a) measured by the mooring array, Seagliders, and PIES were associated with pairs of cyclonic and anticyclonic eddies.

Water Mass Properties

Kuroshio water properties change as the current flows northward (Mensah et al., 2014). Originating as the northward branch of the bifurcation of the NEC, the Kuroshio also interacts with westward-propagating eddies carrying Western Philippine Sea (WPS) water. Gordon et al. (2014) suggest that the Kuroshio east of Luzon Island consists primarily of NEC and WPS waters. The water mass within Lamon Bay (LMB) is a mixture of NEC and WPS waters; the ratio varies with the NEC bifurcation latitude. Our experiment site was located on a channel where South China Sea (SCS) water may intrude into the WPS, as observed and reported by Gordon et al. (2014).

The Seaglider sections with simultaneous high-vertical-resolution measurements of temperature, salinity, and geostrophic current are used to determine Kuroshio water mass properties. Temperature–salinity (T-S) analysis is used to remove the vertical heaving influence of internal waves. The mean meridional geostrophic current, temperature, and salinity measurements from 15 Seaglider sections are plotted on the T-S diagram (Figure 4). The meridional geostrophic currents computed by Seaglider measurements are shown on the T-S diagram (Figure 4a). T-S properties of the NEC, the WPS, and the SCS are computed using historical Argo float data (<http://www.argo.ucsd.edu>) collected between 1998 and 2014 and averaged over the areas defined in Figure 1. The meridional component of the geostrophic current derived from Seaglider measurements is also averaged in time and in isopycnal layers (Figure 5a). The northward transport is averaged in isopycnal layers (Figure 5b). The salinity with the maximum transport on density layers is shown in Figure 5d (yellow dots).

The northward Kuroshio and the southward LU are separated by the isopycnal surface $\sigma_\theta = 26.75 \text{ kg m}^{-3}$ (Figures 4a and 5a), which corresponds to the salinity minimum of the NPIW (Mensah

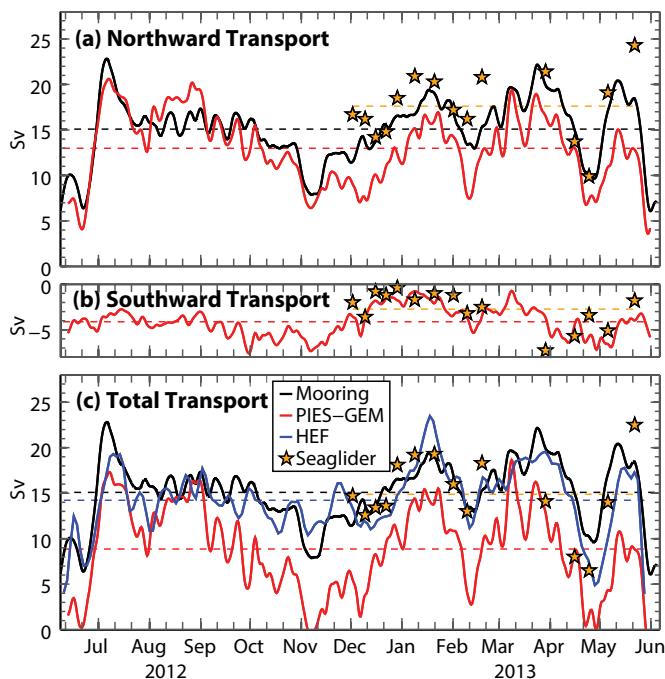


FIGURE 3. Two-day low-pass filtered time series of depth integrated (a) Kuroshio transport, where Kuroshio is defined as the northward flow, (b) Luzon Undercurrent (LU) transport, where LU is defined as the southward flow below the Kuroshio, and (c) total transport across the observational sections. The black curve, yellow stars, and red curve represent the results from the moored array, Seaglider, and PIES, respectively. The blue curve in (c) shows the total transport computed from HPIES. Note that the maximum extrapolated depth for mooring measurements is 600 m, and the maximum

depth for Seaglider measurements is 1,000 m. Horizontal dashed lines represent the mean transports averaged over the observational periods, color coded for different platforms.

et al., 2015; Figure 5c). The NPIW originates from high-latitude, low-salinity water that is subducted and spread in the North Pacific Ocean.

Two distinct types of northward-flowing water masses are present in the upper layer at $\sigma_\theta < 24 \text{ kg m}^{-3}$ (Figure 4a,b). The relatively low salinity, < 34.4 , type of the northward-flowing water located in the shallow west flank of the Kuroshio (Figures 4c and 5c labeled as “low S”) represents the northward-flowing SCS water, likely entrained from the Babuyan channel, west of the moored array. This SCS water is restricted to a shallow layer, $< 20 \text{ m}$ (Figure 4c), and represents a negligible value of the total Kuroshio transport (Figure 4b). The relatively high-salinity water type of the northward current in the upper layer at $\sigma_\theta < 24 \text{ kg m}^{-3}$ is located within the Kuroshio core (Figures 4a and 5c) and has a broad range of T-S properties encompassing NEC and WPS waters. Note that T-S properties of NEC and WPS waters in the layer $24.5 \text{ kg m}^{-3} < \sigma_\theta < 26.0 \text{ kg m}^{-3}$ are indistinguishable.

Transport was computed at a prescribed T-S grid scale (Figure 4b). Two significant volumes of the northward current exist in a thin layer $21.5 \text{ kg m}^{-3} < \sigma_\theta < 22.5 \text{ kg m}^{-3}$ and a broad layer $22.5 \text{ kg m}^{-3} < \sigma_\theta < 26.8 \text{ kg m}^{-3}$ (Figures 4b and 5b). The upper layer has T-S properties that resemble both NEC and WPS waters, and the northward transport is $\sim 7 \text{ Sv}$ (Figure 5d). The lower layer $22.5 \text{ kg m}^{-3} < \sigma_\theta < 26.0 \text{ kg m}^{-3}$ resembles NEC water, and the northward transport is $\sim 10 \text{ Sv}$. The water mass in the layer $26 \text{ kg m}^{-3} < \sigma_\theta < 26.8 \text{ kg m}^{-3}$ has WPS water properties, and the northward transport is $\sim 1.5 \text{ Sv}$ (Figure 5d), representing the layer of NPIW above its salinity minimum (Figure 5c).

LUZON UNDERCURRENT

The velocity structure of the LU was measured by Seagliders and PIES. The annual mean geostrophic component of meridional velocity estimated by Seagliders reveals a robust southward current

between 122°E and 123°E , with a maximum southward velocity of -0.1 m s^{-1} located around 122.5°E , east of the shelf break (Figure 2a). The LU geostrophic current computed from PIES data (not shown) is in good agreement with that from Seagliders.

LU transport is computed by integrating the southward current from the base

of the Kuroshio to the 1,000 m maximum depth of Seaglider geostrophic current measurements and integrating to 1,000 m, the deepest reliable depth for the geostrophic current measurements, from PIES (Figure 3b). LU transport estimates from the two platforms have similar temporal variations. LU southward transport is the weakest, $\sim 1.5 \text{ Sv}$,

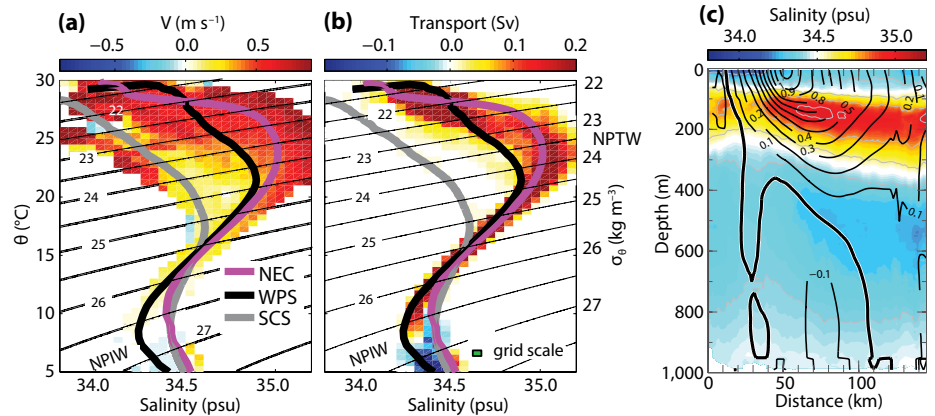


FIGURE 4. Means of (a) meridional velocity and (b) transport on a T-S diagram computed from 15 sections of Seaglider observations. The thick magenta, thick black, and thick gray curves represent T-S properties of NEC, WPS, and SCS waters. Isopycnal surfaces are labeled. Panel (c) shows the mean salinity averaged over 15 Seaglider sections. Black curves indicate meridional velocity isotachs. The green box, labeled grid scale, in panel (b) represents the area of the temperature and salinity grid size used to compute the transport. The North Pacific Intermediate Water (NPIW) and North Pacific Tropical Water (NPTW) are labeled in (a) and (b).

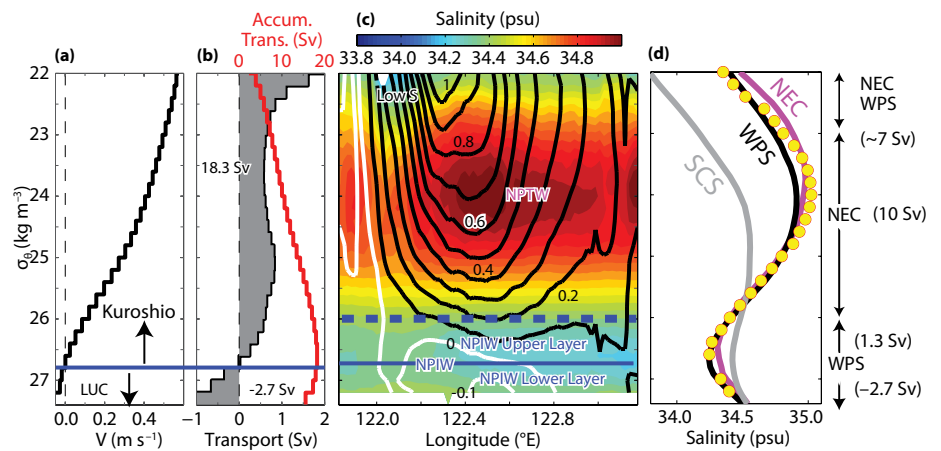


FIGURE 5. Temporal mean of Seaglider estimates of (a) meridional geostrophic current, (b) northward transport (shading), and the accumulated transport from the surface (red). The total transports of the Kuroshio (18.3 Sv) and the Luzon Undercurrent (-2.7 Sv) are labeled in (b). (c) Salinity on the isopycnal coordinate. Black and white contour lines represent northward and southward velocity isotachs. The solid horizontal blue line marks the isopycnal surface dividing the northward-flowing Kuroshio and the southward-flowing Luzon Undercurrent and also the center of the low-salinity North Pacific Intermediate Water (NPIW). The high-salinity North Pacific Tropical Water (NPTW) is labeled in (c). The low-salinity SCS water west of the Kuroshio is labeled as “Low S.” The blue horizontal dashed line in (c) represents the upper bound of the NPIW upper core. (d) Salinity properties of the NEC (magenta), WPS (black), and SCS (gray). Yellow circles indicate the salinity where the maximum transport is present on each isopycnal layer observed by Seagliders. The water mass properties and transports are summarized on the right side of panel (d).

from December 2012 to January 2013, and the strongest, 6–8 Sv, at the end of March 2013. Averaged over the observational period, LU transport has a mean of -2.7 Sv and a standard deviation of 2 Sv computed from Seaglider measurements,

current transport is due to Kuroshio transport variation in the upper 600 m and that LU transport is relatively weak and stable. The transport is 14.1 ± 4.4 Sv measured by HPIES, 14.9 ± 4.2 Sv estimated by Seagliders, and 8.9 ± 5.0 Sv esti-

thus provide a useful realization of the circulation at an earlier time.

The MITgcm-OKMC model setup, state estimation procedure, and model first-guess controls are described in Qiu et al. (2015, in this issue) and Schönau et al. (2015, in this issue). The state estimation adjusts the MITgcm model trajectory to obtain an optimized match with the observations within uncertainty bounds that include satellite-derived along-track SSH separated into temporal mean and anomalies from three satellites: Jason-1 (J1), Jason-2 (J2), and Envisat (N1) obtained from the Radar Altimetry Database System (RADS, <http://rads.tudelft.nl/rads/index.shtml>). Satellite gridded sea surface temperatures (SSTs) are obtained from the daily optimally interpolated product derived from the Tropical Rainfall Measuring Mission (TRMM) Microwave Imager (TMI)/Advanced Microwave Scanning Radiometer - Earth Observing System (TMI-AMSR-E), produced by Remote Sensing Systems Inc. (<http://www.remss.com>), and OKMC Spray glider and Argo (obtained from the CORIOLIS data server, <http://www.coriolis.eu.org>) temperature and salinity profiles. Only observations for the period 2010–2011, within the region of interest located at 122°E – 170°E and 5°N – 20°N , were used in the state estimation experiments (excluding the mooring, Seaglider, PIES, and HEF observations discussed here). The state estimation experiments with one-month assimilation windows covered January 2010 through December 2011.

The MITgcm-OKMC assimilated model solutions of the western boundary current for the period 2010–2011 yield mean meridional velocity at the mooring location (Figure 2). The modeled Kuroshio surface currents with magnitude > 1.0 m s $^{-1}$ are confined within the upper 50 m and centered around 122.4°E (Figure 2b). The model also shows the LU below 600 m with a maximum value of -0.1 m s $^{-1}$, centered around 800 m and 122.5°E . These features are qualitatively in agreement with observations. The

“ Although the current study presents robust kinematic features of the western boundary current using measurements taken from various platforms, the observational period is only one year short and the dynamics are not studied. ”

and a mean of -4.1 Sv and a standard deviation of 1.7 Sv from PIES measurements. Despite averaging over different periods, the mean transports and standard deviations from these two independent measurements are in good agreement. The LU transports the layer of NPIW below its salinity minimum southward (Figures 4b and 5c–d).

BAROTROPIC TRANSPORT OF THE WESTERN BOUNDARY CURRENT

The HEF measurements were used to compute the averaged horizontal currents over the entire water column. The transport of the western boundary current integrated over the full ocean depth, called the barotropic transport, is computed by integrating the HEF measured full-ocean-depth averaged horizontal current across the HPIES array (Figure 3c). Other estimates of barotropic transport are computed from the observational depth ranges of Seagliders (0–1,000 m), PIES (0–1,000 m), and moorings (0–600 m), and they have similar temporal variations, reflecting that the primary temporal variation of the western boundary

transport is due to Kuroshio transport variation in the upper 600 m and that LU transport is relatively weak and stable. The transport is 14.1 ± 4.4 Sv measured by HPIES, 14.9 ± 4.2 Sv estimated by Seagliders, and 8.9 ± 5.0 Sv estimated by PIES. The barotropic transport estimated from HPIES and Seagliders are statistically indistinguishable and support the estimate of -2.7 Sv for LU transport from Seaglider measurements.

NUMERICAL MODEL SIMULATIONS

Modeling was used to provide a space-time context for the OKMC observations, offering realistic realizations of the regional circulation and a broader regional analysis for tracing possible water transport pathways. The series of one-month ocean state estimates calculated for the period 2010–2011 using the MIT general circulation model (MITgcm; Marshall et al., 1997) provides a dynamically consistent representation of the circulation, although the time range does not match that of observations presented here and the model topography cannot match the true topography. While the MITgcm state estimates cannot be validated directly against the moorings and the Seagliders, they do fit the altimeter, Argo, and Spray glider (Sherman et al., 2001) observations and have been cross validated by forecasts (not shown), and

rms difference between model velocity and mooring observations in the upper 400 m is 0.18 m s^{-1} and 0.05 m s^{-1} at western and eastern flanks of the Kuroshio, respectively. Also, in a striking model-observation difference in the offshore shift of the Kuroshio maximum current with depth, the shift is greater in the model than in the observations. This is possibly due to unresolved topography west of the Kuroshio that forces the deeper current offshore before it enters Luzon Strait. The large rms difference between model velocity and observations at the western Kuroshio flank (Figure 2) is likely due to the aforementioned unresolved topography. The estimates from the MITgcm-OKMC assimilated model solutions for the Kuroshio, LU, and the total transport have means (and standard deviations) of 15.5 Sv (6.2 Sv), -4.3 Sv (2.5 Sv), and 10.3 Sv (8.9 Sv). Model and observation mean values are similar, especially for the Kuroshio, but standard deviations are greater for the model than for the observations, which is likely due to larger eddy effects and different sampling periods in the model. In agreement

with observations reported in Lien et al. (2014), simulated Kuroshio transport has strong anomalies of $O(10 \text{ Sv})$ in $O(10 \text{ days})$ (not shown). Because of the different time periods for model simulations and observations, direct comparisons cannot be made, but model statistical properties compare reasonably well with the observations and provide an estimate of interannual variability.

The optimized model solutions provide a broad picture of the Kuroshio and LU water mass pathways. The mean estimated salinity and velocities over the period 2010–2011 were plotted on four isopycnal surfaces corresponding to water mass characteristics from observations at the mooring location (Figures 5d and 6). On $\sigma_\theta = 24 \text{ kg m}^{-3}$ (Figure 6a), the northward Kuroshio intermediate flow is drawn mostly from the NPTW in the NEC, whereas lower Kuroshio northward flow with $\sigma_\theta = 26.5 \text{ kg m}^{-3}$ (Figure 6b) is solely drawn from the WPS, above the NPIW salinity minimum. At $\sigma_\theta = 26.75 \text{ kg m}^{-3}$, corresponding to the NPIW salinity minimum, the modeled flow from the WPS diverges around

18°N – 19°N , where the mooring is located (Figure 6c). The LU southward flow at $\sigma_\theta = 27 \text{ kg m}^{-3}$ (Figure 6d) is fed mainly by the WPS, below the NPIW salinity minimum. These optimized model results are consistent with the observed water mass pathways (Figure 5d).

SUMMARY AND DISCUSSION

The velocity structure, transport, and water mass properties of the Kuroshio and the LU east of Luzon Island were observed by four independent platforms simultaneously for nearly one year. The Kuroshio and the LU are permanent features east of Luzon Island. The Kuroshio transport is strongly modulated by westward-impinging eddies, with anomalies up to 10 Sv in $O(10 \text{ days})$ by pairs of cyclonic and anticyclonic eddies. The annual Kuroshio transport is $16 \pm 4 \text{ Sv}$.

Figure 7 summarizes the Kuroshio and LU transports and water mass pathways east of Luzon based on Seaglider measurements. The Kuroshio is composed of a mixture of NEC and WPS waters in a layer above the NPTW with a transport of $\sim 7 \text{ Sv}$. Within the layer between the

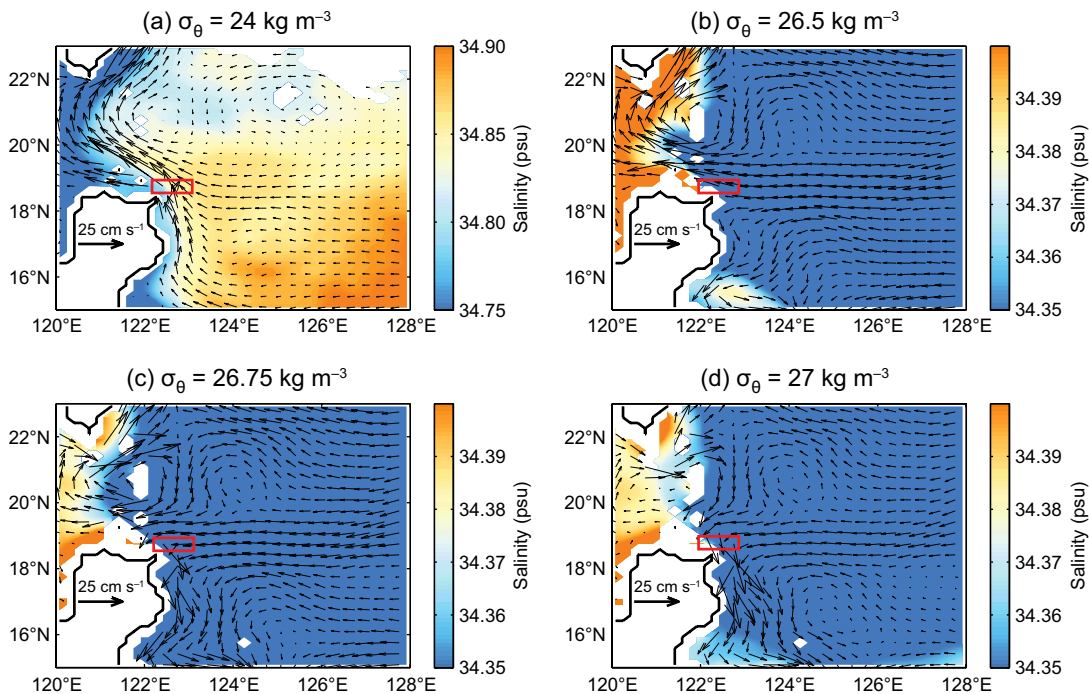


FIGURE 6. Mean salinity and velocity fields on isopycnal coordinates from MITgcm optimized model solutions for the period 2010–2011 on isopycnal surfaces of (a) $\sigma_\theta = 24 \text{ kg m}^{-3}$, (b) $\sigma_\theta = 26.5 \text{ kg m}^{-3}$, (c) $\sigma_\theta = 26.75 \text{ kg m}^{-3}$, and (d) $\sigma_\theta = 27 \text{ kg m}^{-3}$. The red rectangular box represents the OKMC observational site.

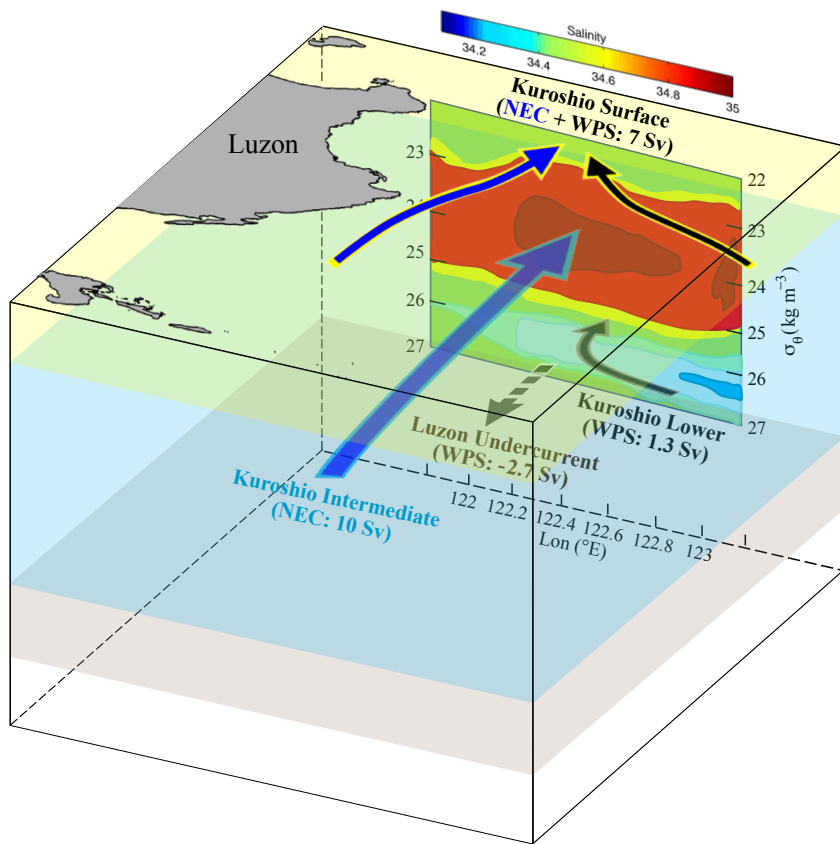



FIGURE 7. Diagram summarizing the transport and sources of water masses of the northward-flowing Kuroshio and the southward-flowing Luzon Undercurrent in potential density and longitude coordinates. The color background represents the salinity section along 18.75°N measured by Seaglider, as shown in Figure 5c. The Kuroshio transport is divided into three layers according to their water masses. The Kuroshio surface layer has a transport of ~7 Sv and consists of water masses from NEC (blue arrow with yellow outline) and WPS (black arrow with yellow outline). The Kuroshio intermediate layer has a transport of 10 Sv and carries water from the NEC (large blue arrow with cyan outline). The Kuroshio lower layer has a transport of 1.3 Sv and consists of water from WPS (solid gray arrow). Luzon Undercurrent transport is about -2.7 Sv and carries water from WPS (dashed gray arrow).

NPTW and the upper layer of the NPIW, Kuroshio transport is ~10 Sv and consists mostly of NEC water. In the lower Kuroshio layer, the transport is ~1.5 Sv and consists of WPS above the salinity minimum of NPIW. Between the base of the Kuroshio and 1,000 m depth, the LU transports WPS waters below the salinity minimum of NPIW southward at ~2.7 Sv. The MITgcm-4D-Var state estimates successfully reproduce the observed Kuroshio and LU transports and the strong Kuroshio transport anomalies caused by impinging anticyclonic/cyclonic eddies. The model also reproduces the observed patterns of Kuroshio and LU velocity structures and transports and confirms the sources of water masses in the Kuroshio and the LU

identified by observations. Although the current study presents robust kinematic features of the western boundary current using measurements taken from various platforms, the observational period is only one year short and the dynamics are not studied. Many scientific questions remain, including the interannual variations of the western boundary current, LU dynamics, the dynamics of eddy-western boundary current interactions, eddy modifications of western boundary current transport and properties, the influence of eddies on the Kuroshio intrusion into the SCS, as well as effects on the ecosystem, for example, the migration of eel larvae carried by the Kuroshio (Aoyama et al., 2014). 

REFERENCES

- Andres, M., S. Jan, T.B. Sanford, V. Mensah, L.R. Centurioni, and J.W. Book. 2015. Mean structure and variability of the Kuroshio from northeastern Taiwan to southwestern Japan. *Oceanography* 28(4):84–95, <http://dx.doi.org/10.5670/oceanog.2015.84>.
- Andres, M., M. Wimbush, J.-H. Park, K.-I. Chang, B.-H. Lim, D.R. Watts, H. Ichikawa, and W.J. Teague. 2008. Observations of Kuroshio flow variations in the East China Sea. *Journal of Geophysical Research* 113, C05013, <http://dx.doi.org/10.1029/2007JC004200>.
- Aoyama, J., S. Watanabe, M.J. Miller, N. Mochioka, and T. Otake. 2014. Spawning sites of the Japanese eel in relation to oceanographic structure and the West Mariana Ridge. *PLoS ONE* 9(2):e88759, <http://dx.doi.org/10.1371/journal.pone.0088759>.
- Centurioni, L.R., P.P. Niiler, and D.-K. Lee. 2004. Observations of inflow of Philippine Sea water into the South China Sea through the Luzon Strait. *Journal of Physical Oceanography* 34:113–121, [http://dx.doi.org/10.1175/1520-0485\(2004\)034<0113:OOIOPS>2.0.CO;2](http://dx.doi.org/10.1175/1520-0485(2004)034<0113:OOIOPS>2.0.CO;2).
- Chang, Y.L., Y. Miyazawa, and X. Guo. 2015. Effects of the STCC eddies on the Kuroshio based on the 20-year JCOPE2 reanalysis results. *Progress in Oceanography* 135:64–76, <http://dx.doi.org/10.1016/j.pocean.2015.04.006>.
- Chave, A.D., and D.S. Luther. 1990. Low frequency, motionally induced electromagnetic fields in the ocean: Part 1. Theory. *Journal of Geophysical Research* 95:7,185–7,200, <http://dx.doi.org/10.1029/JC095iC05p07185>.
- Chern, C.-S., and J. Wang. 2005. Interactions of mesoscale eddy and western boundary current: A reduced-gravity numerical model study. *Journal of Oceanography* 61:271–282, <http://dx.doi.org/10.1007/s10872-005-0037-z>.
- Donohue, K.A., D.R. Watts, K.L. Tracey, A.D. Greene, and M. Kennelly. 2010. Mapping circulation in the Kuroshio Extension with an array of current and pressure recording inverted echo sounders. *Journal of Atmospheric and Oceanic Technology* 27:507–527, <http://dx.doi.org/10.1175/2009JTECHO686.1>.
- Early, J.J., R.M. Samelson, and D.B. Chelton. 2011. The evolution and propagation of quasigeostrophic ocean eddies. *Journal of Physical Oceanography* 41:1,535–1,555, <http://dx.doi.org/10.1175/2011JPO4601.1>.
- Eriksen, C.C., T.J. Osse, R.D. Light, T. Wen, T.W. Lehman, P.L. Sabin, J.W. Ballard, and A.M. Chiodi. 2001. Seaglider: A long-range autonomous underwater vehicle for oceanographic research. *IEEE Journal of Oceanic Engineering* 26(4):424–436, <http://dx.doi.org/10.1109/48.972073>.
- Gordon, A.L., P. Flament, C. Villanoy, and L. Centurioni. 2014. The nascent Kuroshio of Lamon Bay. *Journal of Geophysical Research* 119:4,251–4,263, <http://dx.doi.org/10.1002/2014JC009882>.
- Hansen, D.V., and P.M. Poulain. 1996. Quality control and interpolations of WOCE-TOGA drifter data. *Journal of Atmospheric and Oceanic Technology* 13(4):900–909, [http://dx.doi.org/10.1175/1520-0426\(1996\)013<0900:QCAIOW>2.0.CO;2](http://dx.doi.org/10.1175/1520-0426(1996)013<0900:QCAIOW>2.0.CO;2).
- Hasunuma, K., and K. Yoshida. 1978. Splitting of the subtropical gyre in the western north Pacific. *Journal of the Oceanographic Society of Japan* 34:160–172, <http://dx.doi.org/10.1007/BF02108654>.
- Hu, D., and M. Cui. 1991. The western boundary current of the Pacific and its role in the climate. *Chinese Journal of Oceanology and Limnology* 9(1):1–14, <http://dx.doi.org/10.1007/BF02849784>.
- Hu, D.-X., S.-J. Hu, L.-X. Wu, L. Li, L.-L. Zhang, X.-Y. Diao, Z.-H. Chen, Y.-L. Li, F. Wang, and D.-L. Yuan. 2013. Direct measurements

- of the Luzon Undercurrent. *Journal of Physical Oceanography* 43(7):1,417–1,425, <http://dx.doi.org/10.1175/JPO-D-12-0165.1>.
- Jan, S., Y.-J. Yang, J. Wang, V. Mensah, T.-H. Kuo, M.-D. Chiou, C.-S. Chern, M.-H. Chang, and H. Chien. 2015. Large variability of the Kuroshio at 23.75°N east of Taiwan. *Journal of Geophysical Research* 120:1,825–1,840, <http://dx.doi.org/10.1002/2014JC010614>.
- Johns, W.E., D.R. Watts, and H.T. Rossby. 1989. A test of geostrophy in the Gulf Stream. *Journal of Geophysical Research* 94:3,211–3,222, <http://dx.doi.org/10.1029/JC094iC03p03211>.
- Kim, Y.Y., T. Qu, T. Jensen, T. Miyama, H. Mitsudera, H.-W. Kang, and A. Ishida. 2004. Seasonal and interannual variations of the North Equatorial Current bifurcation in a high resolution OGCM. *Journal of Geophysical Research* 109, C03040, <http://dx.doi.org/10.1029/2003JC002013>.
- Kuo, Y., and C.-S. Chern. 2011. Numerical study on the interactions between a mesoscale eddy and a western boundary current. *Journal of Oceanography* 67:263–272, <http://dx.doi.org/10.1007/s10872-011-0026-3>.
- Lien, R.-C., B. Ma, Y.-H. Cheng, C.-R. Ho, B. Qiu, C.M. Lee, and M.-H. Chang. 2014. Modulation of Kuroshio transport by mesoscale eddies at the Luzon Strait entrance. *Journal of Geophysical Research* 119:2,129–2,142, <http://dx.doi.org/10.1002/2013JC009548>.
- Lumpkin, R., S.A. Grodsky, L. Centurioni, M.-H. Rio, J.A. Carton, and D. Lee. 2013. Removing spurious low-frequency variability in drifter velocities. *Journal of Atmospheric and Oceanic Technology* 30(2):353–360, <http://dx.doi.org/10.1175/jtech-d-12-00139.1>.
- Marshall, J., A. Adcroft, C. Hill, L. Perelman, and C. Heisey. 1997. A finite-volume, incompressible Navier Stokes model for studies of the ocean on parallel computers. *Journal of Geophysical Research* 102(C3):5,753–5,766, <http://dx.doi.org/10.1029/96JC02775>.
- Maximenko, N., R. Lumpkin, and L. Centurioni. 2013. Ocean surface circulation. *International Geophysics* 103: 283–304, <http://dx.doi.org/10.1016/B978-0-12-391851-2.00012-X>. (Special issue on Ocean Circulation and Climate: A 21st Century Perspective. G. Siedler, S.M. Griffies, J. Gould, and J.A. Church, eds.)
- Meinen, C.S., D.S. Luther, D.R. Watts, K.L. Tracey, A.D. Chave, and J. Richman. 2002. Combining inverted echo sounder and horizontal electric field recorder measurements to obtain absolute velocity profiles. *Journal of Atmospheric and Oceanic Technology* 19:1,653–1,664, [http://dx.doi.org/10.1175/1520-0426\(2002\)019<1653:CIESA>2.0.CO;2](http://dx.doi.org/10.1175/1520-0426(2002)019<1653:CIESA>2.0.CO;2).
- Meinen, C.S., and D.R. Watts. 2000. Vertical structure and transport on a transect across the North Atlantic Current near 42°N: Time series and mean. *Journal of Geophysical Research* 105:21,869–21,892, <http://dx.doi.org/10.1029/2000JC900097>.
- Mensah, V., S. Jan, M.-H. Chang, and Y.-J. Yang. 2015. Intraseasonal to seasonal variability of intermediate waters along the Kuroshio path east of Taiwan. *Journal of Geophysical Research* 120:5,473–5,489, <http://dx.doi.org/10.1002/2015JC010768>.
- Mensah, V., S. Jan, M.-D. Chiou, T.-H. Kuo, and R.-C. Lien. 2014. Evolution of the Kuroshio tropical water from the Luzon Strait to the east of Taiwan. *Deep Sea Research Part I* 86:68–81, <http://dx.doi.org/10.1016/j.dsr.2014.01.005>.
- Niiler, P.P. 2001. The world ocean surface circulation. Pp. 193–204 in *Ocean Circulation and Climate*. G. Siedler, J. Church, and J. Gould, eds, Academic Press.
- Niiler, P.P., A. Sybrandy, K. Bi, P.M. Poulain, and D. Bitterman. 1995. Measurements of the water-following capability of holey-sock and TRISTAR drifters. *Deep Sea Research Part I* 42:1,951–1,964, [http://dx.doi.org/10.1016/0967-0637\(95\)00076-3](http://dx.doi.org/10.1016/0967-0637(95)00076-3).
- Nitani, H. 1972. Beginning of the Kuroshio. Pp. 129–163 in *Kuroshio: Its Physical Aspects*. H. Stommel and K. Yoshida, eds, University of Tokyo Press, Tokyo.
- Pazan, E.E., and P.P. Niiler. 2001. Recovery of near-surface velocity from undrogued drifters. *Journal of Atmospheric and Oceanic Technology* 18(3):476–489, [http://dx.doi.org/10.1175/1520-0426\(2001\)018<0476:RONSVF>2.0.CO;2](http://dx.doi.org/10.1175/1520-0426(2001)018<0476:RONSVF>2.0.CO;2).
- Qiu, B., and R. Lukas. 1996. Seasonal and interannual variability of the North Equatorial Current, the Mindanao Current and the Kuroshio along the Pacific western boundary. *Journal of Geophysical Research* 101:12,315–12,330, <http://dx.doi.org/10.1029/95JC03204>.
- Qiu, B., D.L. Rudnick, I. Cerovecki, B.D. Cornuelle, S. Chen, M.C. Schönau, J.L. McClean, and G. Gopalakrishnan. 2015. The Pacific North Equatorial Current: New insights from the origins of the Kuroshio and Mindanao Currents (OKMC) Project. *Oceanography* 28(4):24–33, <http://dx.doi.org/10.5670/oceanog.2015.78>.
- Qu, T.D., T. Kagimoto, and T. Yamagata. 1997. A subsurface countercurrent along the east coast of Luzon. *Deep Sea Research Part I* 44:413–423, [http://dx.doi.org/10.1016/S0967-0637\(96\)00121-5](http://dx.doi.org/10.1016/S0967-0637(96)00121-5).
- Qu, T., and R. Lukas. 2003. The bifurcation of the North Equatorial Current in the Pacific. *Journal of Physical Oceanography* 33:5–18, [http://dx.doi.org/10.1175/1520-0485\(2003\)033<0005:TBOTNE>2.0.CO;2](http://dx.doi.org/10.1175/1520-0485(2003)033<0005:TBOTNE>2.0.CO;2).
- Qu, T., H. Mitsudera, and T. Yamagata. 1998. On the western boundary currents in the Philippine Sea. *Journal of Geophysical Research* 103:7,537–7,548, <http://dx.doi.org/10.1029/98JC00263>.
- Rudnick, D.L., S. Jan, L. Centurioni, C.M. Lee, R.-C. Lien, J. Wang, D.-K. Lee, R.-S. Tseng, Y.Y. Kim, and C.-S. Chern. 2011. Seasonal and mesoscale variability of the Kuroshio near its origin. *Oceanography* 24(4):52–63, <http://dx.doi.org/10.5670/oceanog.2011.94>.
- Sanford, T.B. 1971. Motional induced electric and magnetic fields in the sea. *Journal of Geophysical Research* 76(15):3,476–3,492, <http://dx.doi.org/10.1029/JC076i015p03476>.
- Schönau, M.C., D.L. Rudnick, I. Cerovecki, G. Gopalakrishnan, B.D. Cornuelle, J.L. McClean, and B. Qiu. 2015. The Mindanao Current: Mean structure and connectivity. *Oceanography* 28(4):34–45, <http://dx.doi.org/10.5670/oceanog.2015.79>.
- Sherman, J., R.E. Davis, W.B. Owens, and J. Valdes. 2001. The autonomous underwater glider “Spray.” *IEEE Journal of Oceanic Engineering* 26:437–446, <http://dx.doi.org/10.1109/48.972076>.
- Sun, C., and D.R. Watts. 2001. A circumpolar gravest empirical mode for the Southern Ocean hydrography. *Journal of Geophysical Research* 106(C2):2,833–2,855, <http://dx.doi.org/10.1029/2000JC900112>.
- Sverdrup, H.U. 1942. *Oceanography for Meteorologists*. Prentice Hall, New York, 246 pp.
- Talley, L.D., 1993. Distribution and formation of North Pacific Intermediate Water. *Journal of Physical Oceanography* 23:517–537, [http://dx.doi.org/10.1175/1520-0485\(1993\)023<0517:DAFONP>2.0.CO;2](http://dx.doi.org/10.1175/1520-0485(1993)023<0517:DAFONP>2.0.CO;2).
- Talley, L.D., G.L. Pickard, W.J. Emery, and J.H. Swift. 2010. *Descriptive Physical Oceanography: An Introduction*, 6th ed. Elsevier, 560 pp.
- Watts, D.R., X. Qian, and K.L. Tracey. 2001. Mapping abyssal current and pressure fields under the meandering Gulf Stream. *Journal of Atmospheric and Oceanic Technology* 18:1,052–1,067, [http://dx.doi.org/10.1175/1520-0426\(2001\)018<1052:MACAPF>2.0.CO;2](http://dx.doi.org/10.1175/1520-0426(2001)018<1052:MACAPF>2.0.CO;2).
- Watts, D.R., and H.T. Rossby. 1977. Measuring dynamic heights with inverted echo sounders: Results from MODE. *Journal of Physical Oceanography* 7:345–358, [http://dx.doi.org/10.1175/1520-0485\(1977\)007<0345:MDHWIE>2.0.CO;2](http://dx.doi.org/10.1175/1520-0485(1977)007<0345:MDHWIE>2.0.CO;2).
- Yang, J., X. Lin, and D. Wu. 2013. On the dynamics of the seasonal variation in the South China Sea throughflow transport. *Journal of Geophysical Research* 118:1–13, <http://dx.doi.org/10.1002/2013JC009367>.
- Yang, K.-C., J. Wang, C.M. Lee, B. Ma, R.-C. Lien, S. Jan, Y.-J. Yang, and M.-H. Chang. 2015. Two mechanisms cause dual velocity maxima in the Kuroshio east of Taiwan. *Oceanography* 28(4):64–73, <http://dx.doi.org/10.5670/oceanog.2015.82>.
- Yang, Y., C.-T. Liu, J.-H. Hu, and M. Koga. 1999. Taiwan Current (Kuroshio) and impinging eddies. *Journal of Oceanography* 55:609–617, <http://dx.doi.org/10.1023/A:1007892819134>.
- Yaremchuk, M., and T. Qu. 2004. Seasonal variability of the large-scale currents near the coast of the Philippines. *Journal of Physical Oceanography* 34(4):844–855, [http://dx.doi.org/10.1175/1520-0485\(2004\)034<0844:SVOTLC>2.0.CO;2](http://dx.doi.org/10.1175/1520-0485(2004)034<0844:SVOTLC>2.0.CO;2).

ACKNOWLEDGMENTS

This work was supported by the US Office of Naval Research (N00014-10-1-0273 and N00014-15-1-2285 to BDC, N00014-10-1-0273 to GG, N00014-14-1-0065 to ALG, N00014-10-1-0468 to TBS, N0001-10-1-0273 to LRC, N00014-10-1-0308 to CML, N00014-10-1-0397 and N00014-10-1-0273 to BM, N00014-10-1-0397 to RCL, and N00014-10-1-0268 to SRJ) and the Taiwan Ministry of Science and Technology. Yang, Chang, and Mensah are supported by the Taiwan Ministry of Science and Technology. We thank the officers and crew of R/V *Roger Revelle* for their assistance with the fieldwork. We especially thank W.-H. Her and graduate students from National Taiwan University and University of the Philippines for help with the mooring, shipboard CTD, and Seaglider operations. The altimeter products used in this analysis were produced by Salto/Duacs and distributed by AVISO, with support from CNES (<http://www.aviso.oceanobs.com/duacs>). Argo data were collected and made freely available by the International Argo Program and the national programs that contribute to it (<http://www.argo.ucsd.edu>, <http://argo.jcommops.org>). The Argo Program is part of the Global Ocean Observing System.

AUTHORS

Ren-Chieh Lien (lien@apl.washington.edu) is Senior Principal Oceanographer and Affiliate Professor, **Barry Ma** is Senior Oceanographer, **Craig M. Lee** is Senior Principal Oceanographer and Associate Professor, and **Thomas B. Sanford** is Senior Principal Oceanographer Emeritus and Professor Emeritus, all at the Applied Physics Laboratory, University of Washington, Seattle, WA, USA. **Vigan Mensah** is a PhD candidate at the Institute of Oceanography, National Taiwan University, Taipei, Taiwan. **Luca R. Centurioni** is Associate Researcher, **Bruce D. Cornuelle** is Research Oceanographer, and **Ganesh Gopalakrishnan** is Project Scientist, all at Scripps Institution of Oceanography, University of California, San Diego, La Jolla, CA, USA. **Arnold L. Gordon** is Professor, Lamont-Doherty Earth Observatory, Columbia University, Palisades, New York, USA. **Ming-Huei Chang** is Assistant Professor, Institute of Oceanography, National Taiwan University, Taipei, Taiwan. **Steve R. Jayne** is Senior Scientist, Woods Hole Oceanographic Institution, Woods Hole, MA, USA. **Yiing Jang Yang** is Associate Professor, Institute of Oceanography, National Taiwan University, Taipei, Taiwan.

ARTICLE CITATION

Lien, R.-C., B. Ma, C.M. Lee, T.B. Sanford, V. Mensah, L.R. Centurioni, B.D. Cornuelle, G. Gopalakrishnan, A.L. Gordon, M.-H. Chang, S.R. Jayne, and Y.J. Yang. 2015. The Kuroshio and Luzon Undercurrent east of Luzon Island. *Oceanography* 28(4):54–63, <http://dx.doi.org/10.5670/oceanog.2015.81>.